Available online at www.sciencedirect.com
ScienceDirect
Applied Surface Science 253 (2007) 3083–3092
applied surface science
www.elsevier.com/locate/apsusc

Effect of fluence on the discoloration of marble cleaned with UV lasers

Jie Zhang [a,*], Andrew J. Birnbaum [a], Y. Lawrence Yao [a], Fen Xu [b], John R. Lombardi [b]

[a] Department of Mechanical Engineering, Columbia University, New York, NY 10027, United States
[b] Department of Chemistry, City College of New York, New York, NY 10031, United States

Received 29 March 2006; accepted 26 June 2006
Available online 1 August 2006

Abstract

The effect of fluence level on the discoloration of marble surfaces after the removal of the encrustation by 355 nm laser pulses is comparatively studied. Considering the thermochemical reaction possibly occurring in the encrustation during laser irradiation, the mechanism responsible for the discoloration of the cleaned marble surface is analyzed. The reduction of iron oxides by graphite plays a key role in determining the final color of the cleaned marble surface. A two-dimensional laser ablative cleaning model including the reaction heat is applied to calculate the temperature distribution during laser heating. The kinetics of the thermochemical reaction is estimated based on the simulated temperature field. The occurrence of the thermochemical reaction is also verified indirectly with experiments. The marble surfaces before and after laser irradiation are characterized in terms of the chemical components through surface enhanced Raman spectroscopy. The surface color is measured with a chromameter using a 1976 CIE $L^*a^*b^*$ color system. The proposed mechanism is also applied to numerically analyze the severe discoloration of marble cleaned with laser pulses at 1064 nm.

PACS: 42.62.−b; 79.20.Ds

Keywords: Laser cleaning; UV laser; Marble

1. Introduction

Marble, a metamorphic limestone, primarily consists of calcite, a crystalline form of calcium carbonate ($CaCO_3$). Marble is widely used in statues and monuments, as well as a structural material. Its exposure to a sulphur dioxide (SO_2)-polluted atmosphere, particularly in an urban environment, results in a thin layer of black encrustation due to the formation of gypsum ($CaSO_4{\cdot}2H_2O$). Sulphur dioxide from the combustion of fossil fuels readily reacts with the $CaCO_3$ present in the marble to form gypsum. The softer and more water-soluble gypsum is easily contaminated by soot particles containing metal oxide and graphite, as well as numerous organic constituents, further contributing to the generation of the black encrustation [1].

This encrustation has a detrimental effect on the aesthetic value of both artistic and practical marble structures. Moreover, the encrustation facilitates the biodeterioration of the marble since it can host bacteria, lichen, mosses, higher plants and other microorganisms [2]. Chemical cleaning is the traditional means for removing the encrustation. However, there exists the possibility of chemical reactions between the chemical agents utilized and marble, as well as the environmental pollution. The encrustation is also mechanically removed through using a scalpel or the air-abrasive machine. The effectiveness of the scalpel is restricted by the restorative talents of the restorer and the brittleness of the material. The results of air-abrasive machine treatments are also largely dependent on the restorer's skill levels, as the machine cannot distinguish the encrustation from the stone. Due to the non-uniformity of the encrustation, unavoidable surface damage of the marble results in the loss of fine details of the artworks [3].

Pulsed laser removal of the encrustation is a promising alternative due to the fast and non-contact operation and the high-precision spatial and temporal control. In addition, the laser pulses cannot damage the marble surface after the removal

* Correspondence to: Columbia University, Department of Mechanical Engineering, Foundation School of Engineering and Applied Science, 220 Mudd Bldg., MC4703 New York, NY 10027, United States. Tel.: +1 212 666 2393; fax: +1 212 666 2393.
E-mail address: jz2112@columbia.edu (J. Zhang).

0169-4332/$ – see front matter © 2006 Elsevier B.V. All rights reserved.
doi:10.1016/j.apsusc.2006.06.056

of the encrustation due to the large difference in the absorptivity between the encrustation and the marble, which is termed self-limiting [3]. Laser cleaning nano-particles from semiconductor surfaces [4] and surface layer from metals or semiconductors [5] have been extensively studied. Since the pulsed laser cleaning of the encrustation from the marble was first implemented by John Asmus in 1971 [6], massive investigations related to the laser cleaning of stoneworks have been performed.

Laboure et al. [7] explored the effect of laser fluence, spot area and water spraying on the cleaning rate of the stone. Siano et al. [8] studied how pulse duration affects the laser stone-cleaning process. Siano et al. [9] also experimentally determined the fluence thresholds corresponding to the various side effects in laser stone cleaning. Laser-induced breakdown spectroscopy (LIBS) was employed as an in situ technique for monitoring the laser removal of the encrustation by Maravelaki et al. [10]. Rodriguez-Navarro et al. [11] found that the marble surface was roughened by the excessive laser pulses at supposedly safe fluence levels.

Both Maravelaki-Kalaitzaki et al. [12] and Marakis et al. [13] comparatively investigated the removal of different types of encrustation with different wavelengths. While the prominent self-limiting effect at 1064 nm is extremely beneficial in protecting the marble surface, the cleaned marble surface becomes severely yellowed. On the contrary, no severe yellowing occurs on the marble surface cleaned at 355 nm.

Klein et al. [14] and Potgieter-Vermaak et al. [15] both postulated that the yellowing at 1064 nm is due to residues of iron oxides on the marble surface detected by their experiments. However, they did not provide an explanation for the presence of these residues. Zafiropulos et al. [16] proposed that the discoloration is mainly an optical phenomenon. The dark particles are vaporized by the IR laser fluences below the cleaning threshold to generate voids in the encrustation. These voids make the light scattering different so that the color perception is altered towards yellow. Nevertheless, this argument lacks evidence.

In the present paper, the influence of the fluence levels on the surface color of marble cleaned with the 355 nm laser pulses is examined. A mechanism leading to the discoloration of the marble surface is proposed based on an analysis of the thermochemical reactions possibly occurring in the encrustation during laser irradiation. A two-dimensional laser ablative cleaning model including the reaction heat of the thermochemical reactions is applied in simulating the temperature field generated by the laser irradiation. Then, the kinetics of the thermochemical reactions are used to verify their presence. The proposed mechanism is also used to explain the severe discoloration of marble cleaned with laser pulses at 1064 nm.

2. Experiment conditions

A Q-switched Nd:YAG laser operating at 355 nm in TEM_{00} mode is used as the light source. The laser has a pulse duration of 50 ns, with a constant repetition rate at 1 kHz. The beam diameter is set at 100 μm and the pulse fluence is varied from 0.3 to 3 J/cm^2 through adjusting the distance of the sample from the focusing lens. The sample is placed on the computer-controlled XYZ stage in open air, while the compressed air blows on the sample to prevent the ablation-formed plasma from touching the focusing lens during the experiment.

Italian white Carrara marble was selected as the investigated sample with dimensions 15 mm × 15 mm × 9 mm. Its surface is honed to eliminate the obvious surface dents. The sample is thoroughly cleaned with methanol before making the encrustation. For numerical calculation of the laser produced temperature field, the encrustation is artificially made to better control the material property. The encrustation is a compound of 5% or 10% hematite (Fe_2O_3) powder, 20% graphite powder and 75% or 70% gypsum ($CaSO_4{\cdot}2H_2O$) (vol.%), mixed with distilled water, and smeared onto the marble with a brush [14]. The marble with the encrustation is then left for 72 h in a storage box. On average, the encrustation thickness is approximately 120 μm.

3. Related thermochemical reactions

3.1. Thermal dehydration and decomposition of gypsum ($CaSO_4{\cdot}2H_2O$)

Gypsum ($CaSO_4{\cdot}2H_2O$, calcium sulphate dehydrate), the major ingredient in the encrustation, is a crystalline mineral that contains about 21% chemically combined water by weight. When gypsum is heated, two thermal dehydration reactions occur starting at 373 and 573 K, respectively. These two reactions are described as:

$$CaSO_4 \cdot 2H_2O \rightarrow CaSO_4 \cdot \tfrac{1}{2}H_2O + \tfrac{3}{2}H_2O - 17.2\,\mathrm{kJ/mol} \quad (1)$$

$$CaSO_4 \cdot \tfrac{1}{2}H_2O \rightarrow CaSO_4 + \tfrac{1}{2}H_2O - 8.6\,\mathrm{kJ/mol} \quad (2)$$

During these two reactions, water is released as steam with an absorbed energy of 81.7 kJ/mol. Therefore, the total required energy in the dehydration of gypsum is 107.5 kJ/mol [17].

At temperatures above 1373 K, $CaSO_4$ starts to decompose into calcium oxide (CaO) and sulphur dioxide (SO_2) according to the following equation [18]:

$$CaSO_4 \rightarrow CaO + SO_2 + \tfrac{1}{2}O_2 - 480\,\mathrm{kJ/mol} \quad (3)$$

Calcite ($CaCO_3$) is dissociated into CaO and carbon dioxide (CO_2) starting at the temperature of 1173–1223 K. The reaction is described as the follows [19]:

$$CaCO_3 \rightarrow CaO + CO_2 - 170\,\mathrm{kJ/mol} \quad (4)$$

3.2. Hematite reduced by solid carbon

When a mixture of hematite (Fe_2O_3) and solid carbon is heated up to the certain temperature, the hematite is reduced into wustite (FeO) at an extremely high rate through two consecutive steps, namely hematite → magnetite (Fe_3O_4) → wustite,

like $Fe_2O_3(s) + C(s) \rightarrow 2FeO(s) + CO$ [20]. Then, two coupled gas–solid reactions take place,

$$FeO + CO \rightarrow Fe + CO_2 \quad (5)$$

$$CO_2 + C \rightarrow 2CO \quad (6)$$

It is known that reaction (5) is catalyzed by the reduced metallic iron. More carbon monoxide (CO) produced in the vicinity of FeO increases the reduction rate of FeO.

If the molten hematite is reduced by solid carbon, the reduction rate rises rapidly. This is termed a smelting reduction. The possible reason is that the molten FeO can more easily contact carbon than solid FeO [21]. The weight volume of FeO is proportional to its reduction rate by solid carbon due to the increased interface area between FeO and carbon [22]. Also, CaO even at the low concentration can significantly expedite this reduction reaction [20]. The catalysis results from the enhanced formation rate of CO through the following redox process:

$$CaO + CO_2 \rightarrow CaO \cdot O + CO \quad (7)$$

$$CaO \cdot O + C \rightarrow CaO + CO \quad (8)$$

The thermochemical reactions introduced above are summarized in Fig. 1. During the laser heating, these thermochemical reactions may occur in the encrustation when the encrustation temperature reaches the reaction-required temperature.

4. Numerical simulation

Laser removal of the encrustation from the marble surface is based on laser ablation. Zhang et al. [5] presented a two-dimensional laser ablative cleaning model, which considers the discontinuity across the Knudsen layer and Stephen boundary at the interface. Through the enthalpy method, the temperature field can be simulated and the resulting phase interfaces identified. In the present paper, the heats of thermochemical reactions occurring in the encrustation are taken into account in the model. When the materials reach the required temperature for the thermochemical reaction, the corresponding reaction heat is integrated into the energy balance equation as:

$$\frac{\partial h}{\partial t} + \frac{\partial \Delta H}{\partial t} = \frac{\partial}{\partial x}\left(\alpha \frac{\partial h}{\partial x}\right) + \frac{1}{r}\frac{\partial}{\partial r}\left(r\alpha \frac{\partial h}{\partial r}\right) \quad (9)$$

where α is heat diffusivity, and x and r are the coordinates along the thickness and radial direction. The enthalpy of the material (heat content of the material) H is expressed as $H = h + \Delta H$, where the sensible heat, $h = c_p T$ (c_p is specific heat, T is temperature) and ΔH is the latent heat of phase change ΔH_P or the reaction heat ΔH_T.

The reaction rate is assumed to follow the Arrhenius law, $k = k_0 \exp(-E/RT)$, where k_0 is the frequency factor, E the activation energy, R the universal gas constant and T is the temperature. Concerning reactions (1) + (2) (dehydration), (3) and (4), the corresponding incorporated reaction heats are calculated as $\Delta H_T = k\,\Delta H_{T0}$, where ΔH_{T0} is the reaction heat, k_0 is assumed to be 6.3×10^{24} [23], 1.32×10^6 [18] and $6.45 \times 10^5\ s^{-1}$ [19], and E is assumed to be 202, 212 and 187 kJ/mol, respectively. Since the mechanism of reactions (5) and (6) is complicated by the co-existence of Fe_2O_3, FeO and Fe, a volume-reaction model is applied in their kinetic analysis [24]. The FeO melting point of 1650 K is viewed as the separation point of the application ranges of two reaction rates. It is assumed that reaction rates follow the first-order kinetic equation,

$$\gamma_{Fe_2O_3} = -k_1[Fe_2O_3] \quad (10)$$

$$\gamma_{FeO(s)} = 2k_1[Fe_2O_3] - k_2[FeO(s)] \quad (T_p < 1650\,K) \quad (11)$$

$$\gamma_{FeO(l)} = 2k_1[Fe_2O_3] - k_2[FeO(l)] \quad (T_p \geq 1650\,K) \quad (12)$$

$$\gamma_{Fe(s\ or\ l)} = k_2[FeO(s)] + k_3[FeO(l)] \quad (13)$$

where k_{10}, k_{20} and k_{30} are assumed to be 600, 1300 and 3400 s^{-1}, respectively. E_1, E_2 and E_3 are assumed to be 50.4, 75.6 and 88.2 kJ/mol, respectively [24].

Total reaction heat is computed in the following manner:

$$\Delta H_T = \Delta H_1 \gamma_{Fe_2O_3} + \Delta H_2 \gamma_{FeO(s)} + \Delta H_3 \gamma_{FeO(l)} \quad (14)$$

where ΔH_1, ΔH_2 and ΔH_3 are the corresponding heats of reaction.

The material parameters of the encrustation are the mass-averaged value of every component. All of the material properties are from Ref. [25]. The calculation domain is chosen as three times the beam diameter in both the radial and depth direction. The absorptivities of the encrustation and marble at 355 nm are assumed to be 0.9 and 0.6, respectively [3].

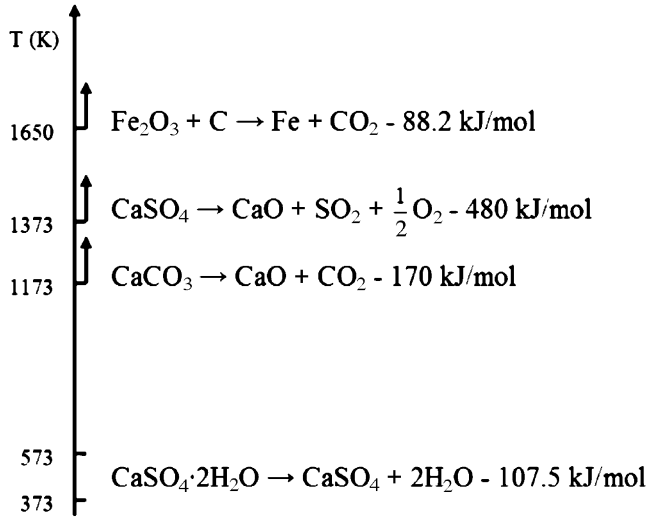

Fig. 1. Schematic of thermochemical reactions taking place in the encrustation during laser heating.

5. Material characterization

The chromameter (Minolta CR-300) is employed to measure the surface color of the marble. In principle, light reflected from the measured surface is simultaneously collected by three photocells, each with spectral sensitivities equal to one of the color matching functions of a special CIE standard observer.

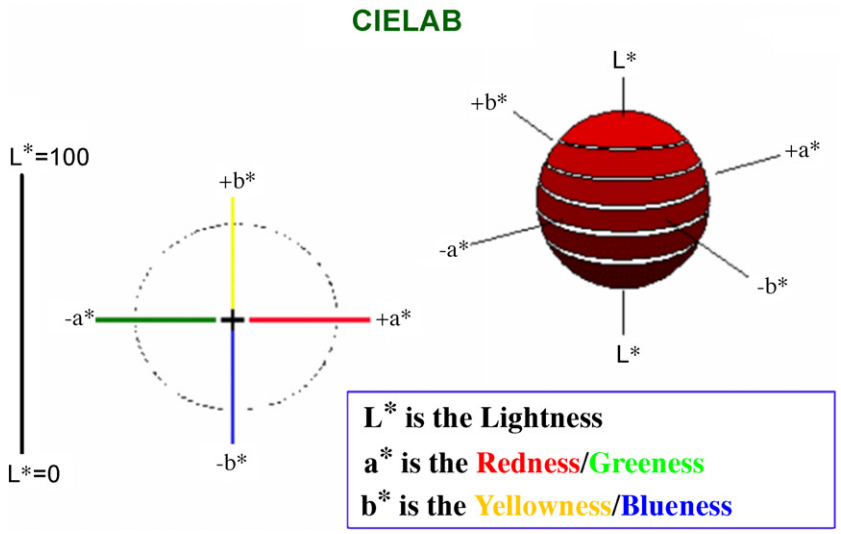

Fig. 2. Schematic of a 1976 CIE $L^*a^*b^*$ color system.

The CR-300 has a measurement spot diameter of 8 mm and use D56 standard xenon light to irradiate the surface. The color measurements are expressed in the perceptually uniform color space, CIE $L^*a^*b^*$ (CIELAB), shown in Fig. 2. The L^* axis is known as the lightness ranging from 0 (black) to 100 (white). The a^* axis and b^* axis represent redness-greenness and yellowness-blueness, respectively. Total color difference ΔE^*_{ab} is defined as $\Delta E^*_{ab} = \sqrt{(\Delta L^*)^2 + (\Delta a^*)^2 + (\Delta b^*)^2}$, where $\Delta L^* = L^* - L^*_t$ describes the lightness change, $\Delta a^* = a^* - a^*_t$ and $\Delta b^* = b^* - b^*_t$ describe the chromaticity change, L^*_t, a^*_t and b^*_t are values of reference white [26].

Surface enhanced Raman spectroscopy (SERS) is used to identify the chemical constituents of the marble surface [27]. When the surface is illuminated by a laser photon, a second photon is scattered. This photon differs in energy from the incipient photon by an energy difference in the levels of the surface constituents. The resulting Raman shift reveals structural information, as well as serving as an analytical tool to identify specific molecular adsorbents. The Raman signals from the surface may be greatly enhanced by application of silver colloid particles on the surface. Raman spectra are excited using a 514 nm CW Argon-ion laser (Spectra-Physics model 2020) at a power of approximately 20 mW. The scattered lines are collected at 90° with a Spex model 1401 double monochromator (resolution ca. 2 cm^{-1}) and detected by an ITT FW-130 photomultiplier (PM) tube with Raman 2005 (software package).

Scanning Electron Microscopy (JEOL) and Scanner (HP Scanjet 5100C) are employed to take the images of cleaned marble surface, respectively. In the case of SEM, the marble surface is coated with silver so that it is electrically conductive.

6. Results and discussions

6.1. Determination of fluence threshold

Successful cleaning is defined as the complete removal of the encrustation without any change of the marble surface in the integrity, structure and color. To experimentally determine the fluence threshold, the sample is irradiated by a single pulse per location. The fluence is continuously increased. When the damage of the encrustation including 5% hematite or the marble is noticeable under the optical microscope, the corresponding fluence values are considered as the thresholds. The experimentally determined thresholds for the encrustation and the marble are 0.45 and 2.5 J/cm^2, respectively.

In order to estimate the accuracy of the proposed numerical model, the fluence threshold is also determined with this model. At 50 ns, the fluence increasing the encrustation surface to the mass-averaged value of the graphite vaporization temperature, the decomposition temperature of hematite and gypsum, namely 2160 K, is considered as its threshold. Similarly, the fluence heating the marble surface to the decomposition temperature of calcite is the threshold for the marble. In Fig. 3, the Raman spectrum of the marble has four bands of $CaCO_3$ at 158, 285, 711 and 1084 cm^{-1} [28]. It is evident that the principal ingredient of the marble is $CaCO_3$.

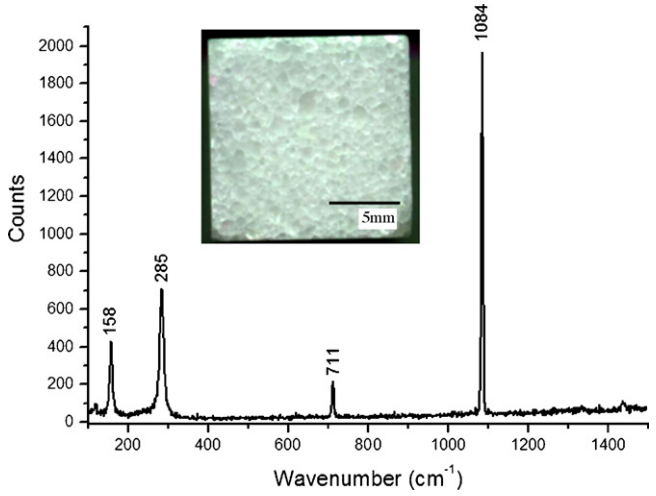

Fig. 3. Raman spectrum and image of white Carrara marble (Raman shifts are excited by the 514 nm laser).

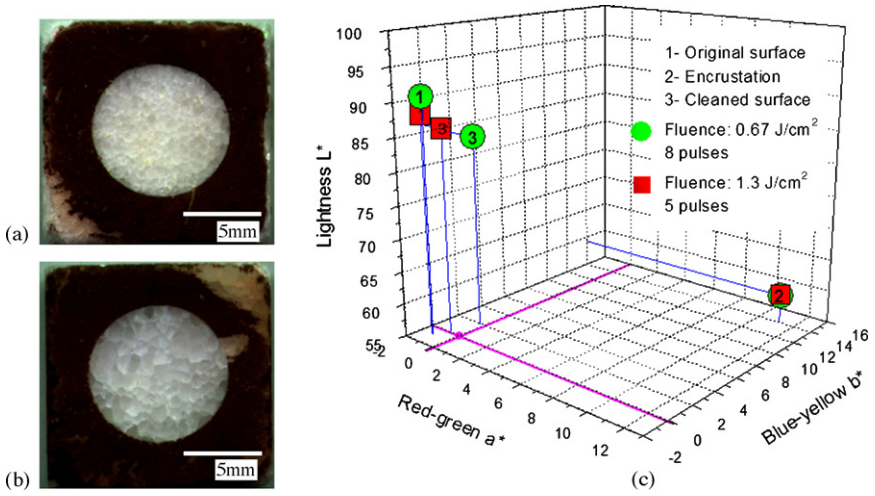

Fig. 4. Images and color measurements of the marble surface before and after the removal of the encrustation with different fluence levels.

The numerically determined thresholds are 0.3 and 1.8 J/cm^2 for the encrustation and the marble, respectively. If the model does not include the thermochemical reaction heat, the determined threshold is 0.12 and 0.42 J/cm^2 for the encrustation and the marble, respectively. The thresholds determined by the model with the reaction heat are more close to the experimental ones, which shows this model is accurate to some extent. The slight overestimate of the model in the ablation effect is possibly because that the heat taken away by the released gases produced in the thermochemical reactions is neglected in the model. Both the experimental and numerical results demonstrate that the threshold difference between the encrustation and the marble is large. This provides marble cleaning at 355 nm, which is self-limiting, thereby avoiding damage to the marble substrate.

6.2. Effect of fluence levels

6.2.1. Experiments

Under the multiple-pulse strategy, the applied laser fluence should be higher than the encrustation threshold of 0.45 J/cm^2 and lower than the marble threshold of 2.5 J/cm^2. Here, the laser fluence is chosen as 0.67 and 1.3 J/cm^2, respectively. Considering the chromameter measurement spot diameter of 8 mm, a circular encrustation area with the diameter of 9 mm is removed. The laser pulses irradiate the encrustation along the circular orbits from the outside to the inside. The pulses have the overlapping rate of 50% to reduce the effect of the Gaussian beam on the irradiation results.

The samples with the encrustation containing 5% hematite are employed in the experiments. Fig. 4(a and b) are the scanned images of the marble cleaned by eight pulses at 0.67 J/cm^2 and five pulses at 1.3 J/cm^2, respectively. The color measurements of the original and cleaned marble surface as well as the encrustation are listed in Table 1. In Fig. 4(c), the color measurements are shown in the 1971 CIE $L^*a^*b^*$ color space. All of color data is the average of five independent measurements.

Compared with the original marble surface, the lightness of the encrustation is much lower, which indicates the black appearance of the encrustation due to the graphite. The positive values of Δa^* and Δb^* denote the encrustation color is inclined to the redness and yellowness owing to the dark-brown hematite in the encrustation.

The lightness of both cleaned marble surfaces are very close to the original ones, which implies the removal of the encrustation. However, the lightness difference between the cleaned and the original surfaces is larger in the case of 0.67 J/cm^2. This reflects the encrustation may not be completely removed. At 1.3 J/cm^2, both of Δa^* and Δb^* are close to the original values and have the same sign. It can be concluded that there is no color variation. At 0.67 J/cm^2, Δa^* is close to the original one and has the same sign. However, Δb^* has a positive sign, which means the surface is becoming slightly yellowed. This phenomenon is referred to as the discoloration of the marble surface.

The Raman spectra of two cleaned surfaces are shown in Fig. 5. The spectrum of the surface irradiated at 1.3 J/cm^2 only shows bands of $CaCO_3$ at 158, 285, 711 and 1084 cm^{-1}. Yet, the spectrum of the surface irradiated at 0.67 J/cm^2 consists of bands of $CaCO_3$ as well as additional bands of Fe_2O_3 at 224 and

Table 1
Color measurements

	Original marble	Encrustation	Marble cleaned by 8 pulses at F = 0.67 J/cm^2	Original marble	Encrustation	Marble cleaned by 5 pulses at F = 1.3 J/cm^2
ΔL^*	90.8433	59.39	84.2767	88.2367	59.39	86.1133
Δa^*	−1.0333	11.2167	−0.20333	−1.19	11.2167	−0.58333
Δb^*	−0.94	13.9633	1.89333	−0.8967	13.9633	−0.0333

ΔL^*: lightness; Δa^*: red-green; Δb^*: blue-yellow.

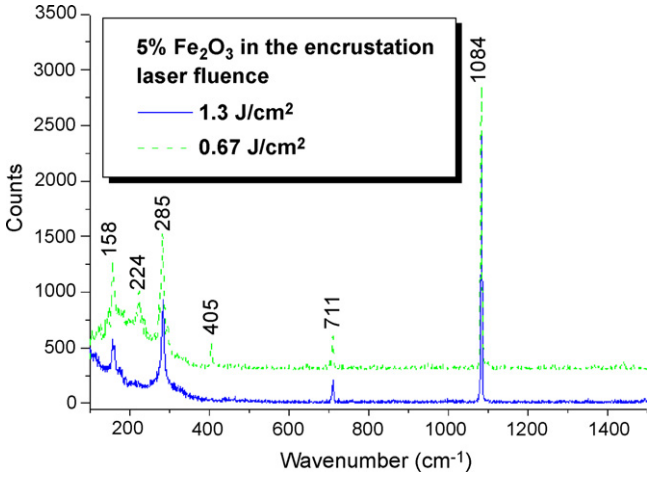

Fig. 5. Raman spectrum of marble surface after the removal of the encrustation with different fluence levels (Raman shifts are excited by 514 nm laser at a power of 20 mW, the green line has an upward shift of 300 for the clarity).

405 cm^{-1} [29]. The $CaCO_3$ bands in two spectra indicate the marble surfaces are exposed after the removal of the encrustation. The Fe_2O_3 bands reflect Fe_2O_3 still resides on the surface irradiated at 0.67 J/cm^2. Thus, it could be deduced that the presence of Fe_2O_3 is related to the surface discoloration. Very small amounts of Fe_2O_3 on the white calcite surface may result in a yellow shift [30]. The SEM pictures of these two cleaned marble surfaces are shown in Fig. 6. Some particles are on the surface cleaned at 0.67 J/cm^2. The surface cleaned at 1.3 J/cm^2 is fairly clean.

6.2.2. *Analysis of the discoloration mechanism*

6.2.2.1. The hematite reduced by the graphite. Fig. 7 shows the simulated history of temperature distribution in the encrustation produced at 1.3 J/cm^2 and the temperature distribution at 50 ns induced by the fluence of 0.67 J/cm^2. Fe_2O_3 and FeO in the grey area are in the molten state due to the temperature ranging between the melting point of Fe_2O_3

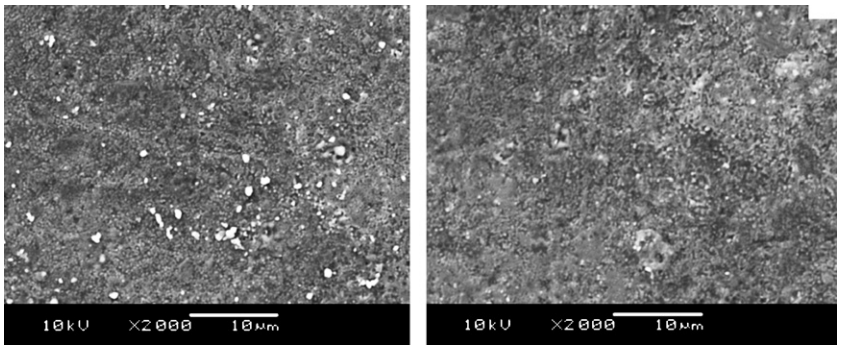

Fig. 6. SEM images of marble surface after the removal of the encrustation with different fluence levels: (a) 0.67 J/cm^2 and (b) 1.3 J/cm^2.

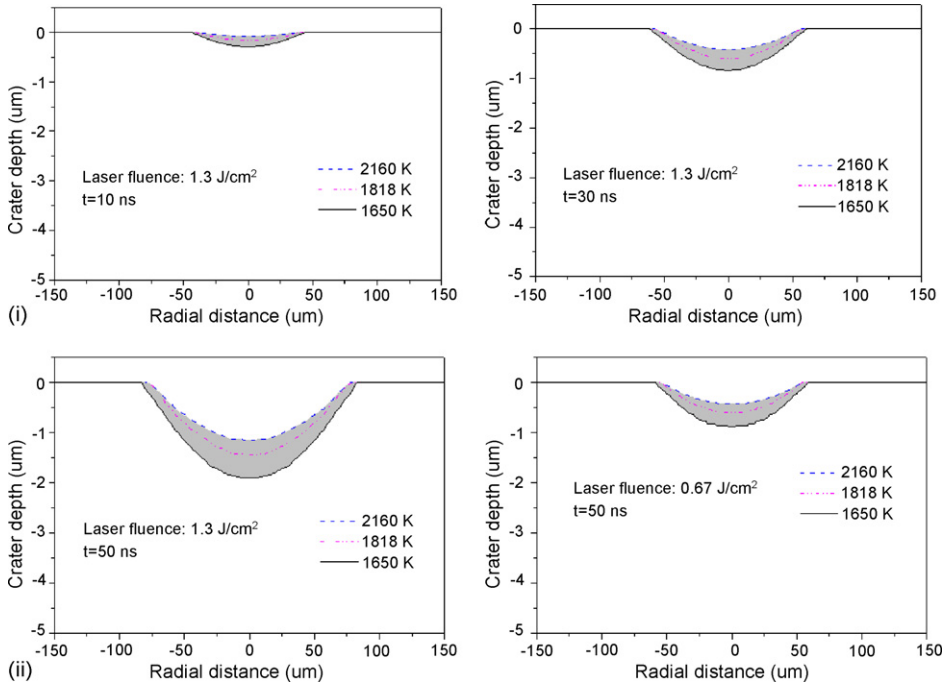

Fig. 7. Simulated time history of temperature distribution in the encrustation produced by the pulse at 1.3 J/cm^2 and the temperature distribution produced by the pulse at 0.67 J/cm^2 at the end of pulse duration 50 ns.

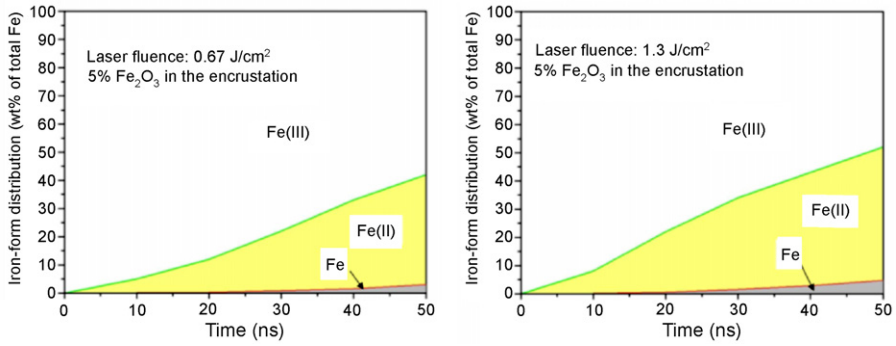

Fig. 8. Simulated iron-form distribution at the end of pulse duration 50 ns with two different fluence levels: (a) 0.67 J/cm^2 and (b) 1.3 J/cm^2.

1818 K and the one of FeO 1650 K. Some graphite powders may contact the molten Fe_2O_3 and FeO because of their random distribution in the encrustation. Correspondingly, part of the molten iron oxides may be reduced by the graphite to produce iron at the very high reaction rate. As mentioned before, this reduction reaction can be considerably accelerated by CaO from the thermal dissociation of $CaSO_4$. In the case of 1.3 J/cm^2, the grey area emerges starting from 10 ns, and is enlarged with the time, which means the smelting reduction of iron oxides may take place during the entire 50 ns. At 0.67 J/cm^2, the grey area at 50 ns suggests the availability of the temperature required by this reaction.

The simulated distribution of Fe, FeO and Fe_2O_3 at 50 ns with the fluence of 0.67 and 1.3 J/cm^2 is shown in Fig. 8. Iron is generated in both cases. The higher the fluence is, the more metallic iron is produced. The evident reason is that the high temperature induced by the high fluence favors the reduction of iron oxides. It should be pointed out that very little hematite is reduced by graphite and the majority of the hematite is ablated by the laser pulse.

Fig. 9 describes the temperature history at the bottom center of the crater generated by three pulses at 1.3 J/cm^2 and six pulses at 0.67 J/cm^2. In the case of 0.67 J/cm^2, iron oxides can be heated above 1000 K by three pulses, respectively. The longer reaction time of the solid iron oxides reduced by the graphite at the high temperature may result in the production of more iron. On the contrary, only one pulse is needed to heat the material above

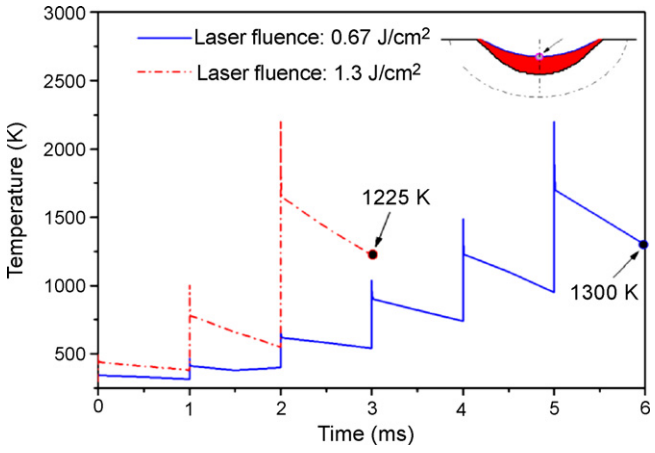

Fig. 9. Simulated time history of temperature at the center of the the final crater bottom irradiated by two different fluence levels.

1000 K in the case of 1.3 J/cm^2. Also, heat accumulation between two successive pulses is enhanced with the pulse number. After three pulses at 1.3 J/cm^2, the temperature is 1225 K; after six pulses at 0.67 J/cm^2, the temperature is 1300 K.

6.2.2.2. The reduced metallic iron during laser irradiation. - During the laser irradiation, the plasma formed impedes the air from interacting with the surface. The dissociation of the ablated hematite in the plasma will produce atomic oxygen [31]. However, oxygen has no solubility in liquid iron, preventing the production of iron oxide at this step [32]. Yet, Pereira et al. [33] experimentally found the appearance of a Fe_2O_3 layer at the iron surface after the irradiation of the XeCl laser. This means that the formation of Fe_2O_3 is due to the chemical reaction between iron and oxygen during the cooling stage. The chemically active iron reacts easily with the oxygen, especially at high temperatures. Since the formation enthalpy of iron oxide is small, iron oxides are produced very near the surface. The iron oxide forms a multilayer scale consisting of FeO, Fe_3O_4 and Fe_2O_3 from the iron bulk to the outermost [34]. Increases in the time that the iron is subjected to high temperatures can lead to increases in the production of iron species in a higher oxidation state, i.e., more Fe_2O_3 is formed.

The majority of iron produced by the current pulse may be taken away by the ablation flux during the next pulse, and the rest of the iron may interact with subsequent pulses. The following investigation focuses on the iron irradiated by the last pulse required by the complete removal of the encrustation, namely the seventh pulse at 0.67 J/cm^2 and the fourth pulse at 1.3 J/cm^2. It is assumed an independent iron particle is irradiated by a single pulse. The 2D ablation model is employed to simulate its temperature distribution [35]. The absorptivity of iron at 355 nm is 0.6 [25]. Considering the heat accumulation, the initial temperature of iron is set as 1225 and 1300 K, as shown in Fig. 9, with the fluence of 1.3 and 0.67 J/cm^2, respectively.

In the case of 1.3 J/cm^2, the temperature in a crater with a depth of 0.22 μm is simulated to be equal or higher than the vaporization point of iron 3134 K, which means the iron can be ablated. Though the actual thickness of the iron left on the marble is difficult to measure, it is certainly relatively minute. Thus, it can be assumed that all of the iron has been ablated. In the case of 0.67 J/cm^2, no iron is simultaneously heated up to 3134 K. The temperature above the melting point of iron

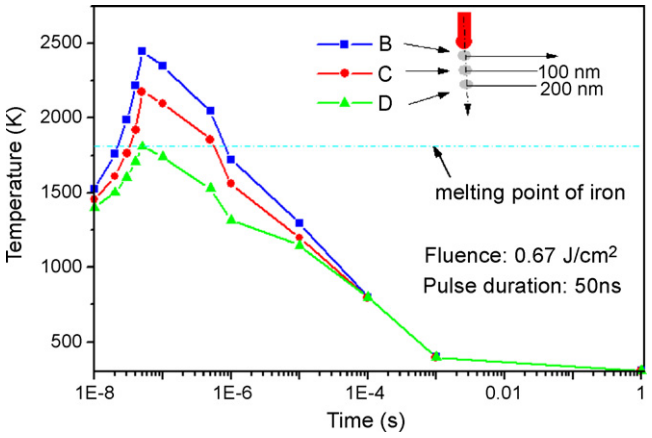

Fig. 10. Simulated temperature history of the points on the iron corresponding to the beam center under the fluence of 0.67 J/cm^2.

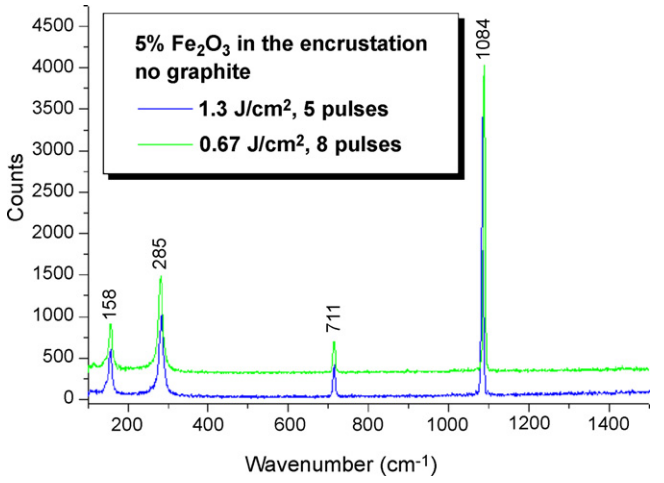

Fig. 11. Raman spectrum of marble surface after the removal of the encrustation without the graphite with different laser fluence levels (Raman shifts are exited by the 514 nm CW laser at a power of 20 mW, the green line has an upward shift of 300 for the clarity).

(1811 K) is in the crater with the depth of 0.4 μm. Thus, the iron is assumed to be just melted.

The simulated temperature history of the points corresponding to the beam center at the different depths in the case of 0.67 J/cm^2 is shown in Fig. 10. It is apparent that the peak temperature is generated at the end of the pulse. The iron could be oxidized during its cooling period of approximately 1 s. Due to the high temperature in the very shallow iron, the iron oxides are in the form of Fe_2O_3. This newly formed Fe_2O_3 may stay at the porous structure of the marble surface because the molten iron may penetrate it during laser irradiation. As extra pulses are incident on the marble, the marble surface temperature is raised very slightly due to its low absorptivity. At this time, the hematite is heated mainly through heat conduction from the marble. Thus, the temperature of hematite may be much lower than its vaporization temperature.

6.3. Effect of graphite

Without graphite, the encrustation consists of 5% hematite and 95% gypsum. The encrustation is irradiated by eight pulses at 0.67 J/cm^2 and five pulses at 1.3 J/cm^2, respectively. The color of original and cleaned marble surfaces as well as the encrustation are measured and listed in Table 2, respectively.

In the case of two fluence levels, the lightness of cleaned surface is very close to its corresponding original value. Meanwhile, two lightness differences between the cleaned and the original surface are almost equal. This probably means the encrustation is completely removed in both cases. Both of Δa^* and Δb^* values are also close to the original ones, and the signs are identical. So, it can be concluded that there is no color variation on the marble surface cleaned at 0.67 and 1.3 J/cm^2. The Raman spectra measured on these two cleaned surfaces are shown in Fig. 11. Both of the Raman spectra are characterized with the bands of $CaCO_3$ (158, 285, 711 and 1084 cm^{-1}). No Fe_2O_3 bands at 224 and 405 cm^{-1} appear. This indicates no Fe_2O_3 exists on two cleaned marble surfaces. Without the graphite, the hematite in the encrustation is just heated, and then ablated. This group of experiments indirectly verifies that

Table 2
Color measurements

	Original marble	Encrustation	Marble cleaned by 8 pulses at F = 0.67 J/cm^2	Original marble	Encrustation	Marble cleaned by 5 pulses at F = 1.3 J/cm^2
ΔL^*	86.5633	66.8067	85.09	87.0067	66.8067	85.67
Δa^*	−1.2933	20.6333	−0.8	−1.057	20.6333	−0.25
Δb^*	−0.7633	10.9733	−0.21	−0.85	10.9733	−0.1933

ΔL^*: lightness; Δa^*: red-green; Δb^*: blue-yellow.

Table 3
Color measurements

	Original marble	Encrustation	Marble cleaned by 8 pulses at F = 0.67 J/cm^2	Original marble	Encrustation	Marble cleaned by 5 pulses at F = 1.3 J/cm^2
ΔL^*	89.3667	57.4067	82.0667	88.2867	57.4067	86.51
Δa^*	−1.3067	19.0167	−0.49667	−1.2833	19.0167	−0.68933
Δb^*	−1.79	13.4667	2.99333	−1.0533	13.4667	0.03

ΔL^*: lightness; Δa^*: red-green; Δb^*: blue-yellow.

hematite is reduced by the graphite to produce iron during laser irradiation.

6.4. Effect of volume weight of hematite

Marble samples are covered with the encrustation containing 10% hematite, 20% graphite and 70% gypsum. These samples are also irradiated by eight pulses at 0.67 J/cm^2 and five pulses at 1.3 J/cm^2, respectively. Table 3 lists the color measurements of original and cleaned marble surfaces as well as the encrustation, respectively.

The color variation of the surfaces cleaned at 0.67 and 1.3 J/cm^2 is similar to the corresponding color measurements shown in Section 6.2.1. The only difference is the value of Δb^* after the irradiation of the pulse at 0.67 J/cm^2. It further shifts towards the positive direction, which means the yellowing of the cleaned surface is aggravated.

Fig. 12 shows the Raman spectra collected from these two cleaned surfaces. Both samples have the $CaCO_3$ bands of 158, 285, 711 and 1084 cm^{-1}. Only the sample irradiated at 0.67 J/cm^2 shows the Fe_2O_3 bands of 224 and 405 cm^{-1}, which indicates the presence of Fe_2O_3 on the marble surface irradiated at 0.67 J/cm^2.

The increased yellowing shift is probably due to the high volume weight of hematite in the encrustation. Lee et al. [22] found that the reduction rate of hematite by graphite rises with the weight of hematite owing to the augmentation of the interface area between hematite and graphite. Therefore, increased iron production results in an increase in the formation of iron oxides. Such experimental results indicate the occurrence of the thermochemical reaction to some extent.

6.5. Analysis of severe yellowing of marble at 1064 nm

In order to explain the severe yellowing of marble cleaned at 1064 nm with the proposed mechanism, the experimental parameters applied in Ref. [14] are adopted in the following analysis. The artificial encrustation contains 20% graphite, 20% hematite and 60% gypsum. The encrustation is removed by 10 or 20 pulses at 0.5 J/cm^2. The pulse duration is 7 ns, and the repetition rate is 2 Hz. In the simulation, the beam size is assumed to be 100 μm in diameter, and the encrustation thickness is 120 μm. The properties of the encrustation are recalculated based on the new ratio of the ingredients.

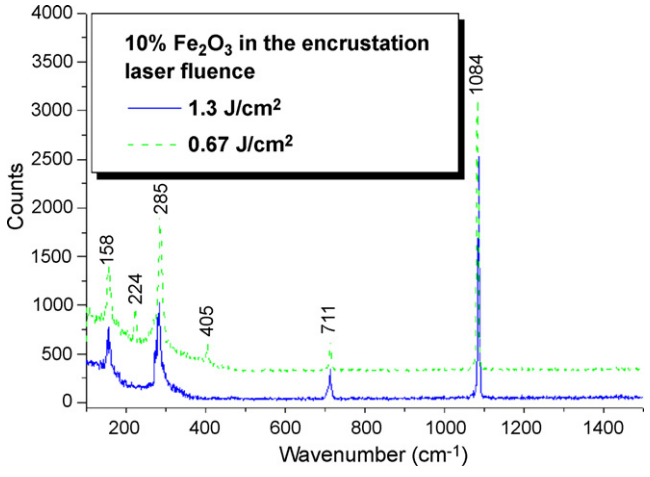

Fig. 12. Raman spectrum of marble surface after the removal of the encrustation with 10% hematite with different laser fluence levels (Raman shifts are excited by the 514 nm CW laser at a power of 20 mW, the green line has an upward shift of 300 for the clarity).

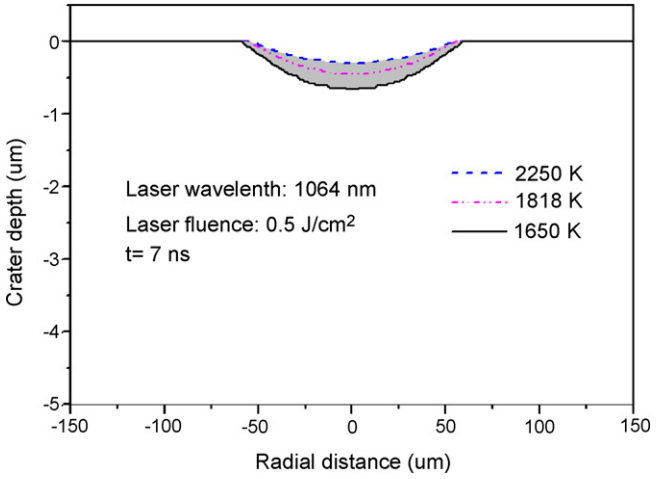

Fig. 13. Simulated temperature distribution in the encrustation produced by a 1064 nm laser pulse with the fluence of 0.5 J/cm^2 at the end of pulse duration 7 ns.

Fig. 13 shows the simulated temperature distribution in the encrustation generated with a fluence of 0.5 J/cm^2 at 7 ns. The ablation temperature of this encrustation is assumed to be 2250 K. Clearly, the temperature in part of the encrustation is in the range from 1818 K (melting point of Fe_2O_3) to 1650 K (melting point of FeO). The smelting reduction of hematite by graphite may take place to form the iron in this area.

Whether iron can be ablated by the last applied pulse in the experiment is related to the final presence of iron on the surface. Therefore, an independent iron particle is assumed to be irradiated by the 10th pulse and the 20th pulse at 0.5 J/cm^2, respectively. The absorptivity of iron at 1064 nm is around 0.31 [25]. Similarly, the initial temperature of iron is numerically calculated to be 700 and 1150 K in the case of the 10th pulse

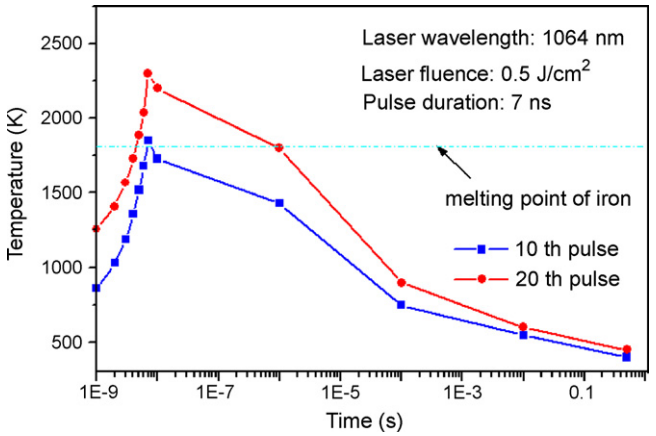

Fig. 14. Simulated temperature history of the point on the iron corresponding to the beam center by the 1064 nm laser pulses.

and the 20th pulse, respectively. The simulated temperature history of the point corresponding to the beam center at the iron surface is shown in Fig. 14. In both cases, the peak temperature is lower than the vaporization temperature of iron 3134 K, which means iron cannot be ablated, just melted. After the pulse is over, the iron requires almost 1 s to cool. Then, the oxygen can react with the high temperature iron to form iron oxides. Hence, the marble surface becomes yellowed. The severe yellowing at 1064 nm may result from the generation of more iron oxide. The marble absorptivity at 1064 nm is only 0.25 [3]. However, the marble absorptivity at 355 nm is slightly higher. The marble-absorbed heat may be helpful in increasing the temperature of the iron to its vaporization point, and hence reducing the amount of the remaining iron and then iron oxide in the case of 355 nm.

7. Conclusions

The fluence levels affect the surface color of marble after the removal of the encrustation by 355 nm laser pulses. During laser irradiation, some hematite is reduced by the graphite to produce iron. High fluence can ablate the iron, but the low fluence just makes the iron melt and remain on the marble. The remaining iron is oxidized by the air right after the laser irradiation. The generated iron oxides are responsible for the light discoloration of the marble surface cleaned with the low fluence. The laser-induced temperature field is calculated with a two-dimensional laser ablative cleaning model including the reaction heat to analyze the kinetics of the thermochemical reactions. With the low fluence, the removal of the encrustation without the graphite does not cause any discoloration to the marble, which indirectly verifies the occurrence of the reduction reaction of hematite by graphite. The higher the volume weight of hematite in the encrustation, the more yellow the marble surface cleaned at low fluence level becomes, which implies an increase in the volume weight of hematite increases the reduction rate of hematite, and then produces more iron. The severe discoloration of marble cleaned at 1064 nm is due to the inability to ablate the iron produced in the reduction of hematite based on the numerical analysis.

Acknowledgements

The authors are grateful to Dr. Mohammad Athar of Columbia University for his permission to access the chromameter. The authors thank Mr. Justin Rasso for his technical assistance during the measurements.

References

[1] T. Skoulikidis, D. Charalambous, Br. Corros. J. 16 (1981) 49.
[2] P.S. Griffin, N. Indictor, R.J. Koestler, Int. Biodeterior. 28 (1991) 187.
[3] M. Cooper, Laser Cleaning in Conservation: An Introduction, Butterworth-Heinemann, 1998.
[4] A.C. Tam, W.P. Leung, W. Zapka, W. Ziemlih, J. Appl. Phys. 71 (7) (1992) 3515.
[5] J. Zhang, Y.W. Wang, P. Cheng, Y.L. Yao, J. Appl. Phys. 99 (6) (2006) 064902.
[6] J.F. Asmus, W. Munk, C. Murphy, Proc. Soc. Photo-Opt. Instrum. 41 (1974) 19.
[7] M. Laboure, P. Bromblet, G. Orial, G. Wiedemann, C. Simon-Boisson, J. Cult. Herit. 1 (2000) s21.
[8] S. Siano, F. Margheri, R. Pini, P. Mazzinghi, R. Salimbeni, Appl. Opt. 36 (27) (1997) 7073.
[9] S. Siano, F. Fabiani, R. Pini, R. Salimbeni, M. Giamello, G. Sabatini, J. Cult. Herit. 1 (2000) s47.
[10] P. Maravelaki, V. Zafiropulos, V. Kilikoglou, M. Kalaitzaki, C. Fotakis, Spectrochim. Acta Part B 52 (1997) 41.
[11] C. Rodriguez-Navarro, A. Rodriguez-Navarro, K. Elert, E. Sebastian, J. Appl. Phys. 95 (7) (2004) 3350.
[12] P. Maravelaki-Kalaitzaki, V. Zafiropulos, C. Fotakis, Appl. Surf. Sci. 148 (1999) 92.
[13] G. Marakis, P. Pouli, V. Zafiropulos, P. Maravelaki-Kalaitzaki, J. Cult. Herit. 4 (2003) 83s.
[14] S. Klein, F. Fekrsanati, J. Hildenhagen, K. Dickmann, H. Uphoff, Y. Marakis, V. Zafiropulos, Appl. Surf. Sci. 171 (2001) 242.
[15] S. Potgieter-Vermaak, R. Godoi, R. Grieken, J. Potgieter, M. Oujja, M. Castillejo, Spectrochim. Acta Part A 61 (2005) 2460.
[16] V. Zafiropulos, C. Balas, A. Manousaki, Y. Marakis, P. Maravelaki-Kalaitzaki, K. Melesanaki, P. Pouli, T. Stratoudaki, S. Klein, J. Hildenhagen, K. Dickmann, B. Luk'Yanchuk, C. Mujat, A. Dogariu, J. Cult. Herit. 4 (2003) 249s.
[17] J.R. Mehaffey, P. Cuerrier, G. Carisse, Fire Mater. 18 (1994) 297.
[18] A. Fuertes, M. Fernandez, Trans. IchemE 73 (Part A) (1995) 854.
[19] W. Lipinski, A. Steinfeld, Int. J. Heat Mass Trans. 47 (2004) 1907.
[20] S.B. Jagtap, A.R. Pande, A.N. Gokarn, J. Chem. Eng. Jpn. 25 (1) (1991) 6.
[21] A. Sato, G. Aragane, K. Kamihara, S. Yoshimatsu, Tetsu-to-Hagane 73 (1987) 812.
[22] J. Lee, D. Min, S. Kim, Metall. Mater. Trans. B 28B (1997) 1019.
[23] D. Fatu, J. Therm. Anal. Calorim. 65 (2001) 213.
[24] K. Sugawara, K. Morimoto, T. Sugawara, AIChE J. 45 (3) (1999) 574.
[25] D.R. Lide, CRC Handbook of Chemistry and Physics, CRC Press, Boca Raton, FL, 2004.
[26] R. Berns, Billmeyer and Saltzman's Principles of Color Technology, John Wiley & Sons Inc., New York, 2000.
[27] R.L. Birke, T.H. Lu, J.R. Lombardi, in: R. Varma, J.R. Selman (Eds.), Techniques for Characterization of Electrodes and Electrochemical Processes, John Wiley & Sons, NY, 1991, p. 211.
[28] M. Prencipe, F. Pascale, C. Zicovich-Wilson, V. Saunders, R. Orlando, R. Dovesi, Phys. Chem. Miner. 31 (2004) 559.
[29] D. Faria, S. Silva, M. Oliveira, J. Raman Spectrosc. 28 (1997) 873.
[30] V. Barro'n, J. Torrent, J. Soil Sci. 37 (1986) 499.
[31] A. Pereira, P. Delaporte, M. Sentis, A. Cros, W. Marine, A. Basillais, A. Thomann, C. Leborgne, N. Semmar, P. Andreazza, T. Sauvage, Thin Solid Films 453–454 (2004) 16.
[32] P. Schaaf, M. Han, K. Lieb, E. Carpene, Appl. Phys. Lett. 80 (6) (2002) 1091.
[33] A. Pereira, A. Cros, P. Delaporte, W. Marine, M. Sentis, Appl. Surf. Sci. 197–198 (2002) 845.
[34] A.S. Khanna, Introduction to High Temperature Oxidation and Corrosion, ASM International, Materials Park, 2002.
[35] W.W. Zhang, Y.L. Yao, K. Chen, Int. J. Adv. Manuf. Technol. 18 (2001) 323.